Synthesis and Characterization of Monetite Prepared Using a Sonochemical Method in a Mixed Solvent System of Water/Ethylene Glycol/*N*,*N*-Dimethylformamide

S. BARADARAN, W.J. BASIRUN, M.R. MAHMOUDIAN, M. HAMDI, and Y. ALIAS

Bioactive monetite (anhydrous calcium hydrogen phosphate, $CaHPO_4$) has been successfully synthesized using the sonochemical method in the presence of a ternary solvent system of water/ethylene glycol (EG)/*N*,*N*-dimethylformamide (DMF). The morphology and chemical composition of the synthesized powders were characterized using field emission scanning electron microscopy, X-ray diffraction, and Fourier transform infrared spectroscopy. The results indicated that with increasing sonication time, the morphology changed slightly from a plate-like one to a combination of plates (flower-like). The formation of flower-like nanosheets requires an optimum time of 40 minutes, and the nanosheets have an average thickness of 210 ± 87 nm. The concentration of DMF clearly influences the morphology and crystal phase of the products. The ideal product was obtained using a water/EG DMF ratio of 1:2.

DOI: 10.1007/s11661-012-1595-5

I. INTRODUCTION

CALCIUM phosphates have been widely investigated as implants for substituting human bone in the field of biomaterials for orthopedics.[1–3] As a bioactive material, under acidic conditions (<4.5), monetite (DCPA, $CaHPO_4$) is one of the stable phases of the calcium phosphates, which have attracted considerable attention.[4] Over the last two decades, several studies have revealed the biomedical applications of bioactive monetite. This material may be used as restorable bone replacement material and a precursor to synthesizing hydroxyapatite, which is an important component of calcium phosphate cement for skeletal repair that is employed in tissue organs, such as the urinary tract and dental stone.[5–9] Therefore, in bio-applications, controlling the morphology of calcium phosphates is crucial because the characteristics of the synthesized powder, such as biocompatibility, bioactivity, stability, and mechanical properties, depend on the structure, morphology, and crystallite size of calcium phosphates.[5]

In addition, throughout the last two decades, calcium phosphates have been synthesized with various morphologies, such as rods,[10,11] plates,[12,13] needles,[14,15] spheres,[16,17] and sheets,[18] which can be controlled by the synthesis conditions. Numerous efforts have been made to synthesize calcium phosphates with different morphologies using diverse methods. The more common techniques include hydrothermal methods,[4,6,11,19,20] solvothermal methods,[21–23] microwave,[24] electro-deposition,[25] sol–gel,[26] emulsion,[16] precipitation from micro-emulsion,[27] crystallization from solution and, in recent years, ultrasonication.[7]

Some reports already exist on the synthesis of monetite. Ma *et al.*[5] reported the synthesis of monetite with a flower-like morphology that consists of nanosheets using a one-step, microwave-assisted method at 368.15 K (95 °C) for 1 hour. Jokic *et al.*[19] synthesized monetite and hydroxyapatite whiskers using a modified hydrothermal method at 433.15 K (160 °C) for 1 hour using urea as a homogeneous precipitation agent. Jinawath *et al.*[6] used the hydrothermal treatment of a monocalcium phosphate monohydrate suspension and lactic acid as a chelating agent to produce monetite whiskers at 433.15 K and 473.15 K (160 °C and 200 °C) for 4 hours. Wei *et al.*[8] reported the synthesis of monetite nanoparticles with various morphologies, such as spheres, nanofibers, and bundles of nanowires, using cetyltrimethylammonium bromide (CTAB) as a surfactant and *n*-pentanol as a co-surfactant. Ruan *et al.*[7] synthesized monetite nanosheets using a sonochemistry-assisted method and reported the effects of ultrasonic irradiation and the CTAB surfactant on the assembly of the monetite nanosheets. This method is extensively used to fabricate nanostructured materials that possess unusual properties,[28] and it has unique reaction effects that are relevant to acoustic cavitation, including the impulsive generation, growth, and collapse of micron-sized bubbles in liquid solutions. Compared to traditional energy sources, high temperatures and pressures occur in the center of the bubbles over a short duration; the high temperatures and pressures are estimated to reach 5000 K (4727 °C) and 1800 atm, respectively. The cooling rate is greater than 10 K/s^{-1} when the bubbles implode.[29,30] The advanta-

S. BARADARAN, PhD Student, is with the Department of Engineering Design and Manufacture, Faculty of Engineering, University of Malaya, 50603 Kuala Lumpur, Malaysia. Contact e-mail: saeid_baradaran@yahoo.com W.J. BASIRUN, Y. ALIAS, Supervisors, and M.R. MAHMOUDIAN, Senior Researcher, are with the Department of Chemistry, Faculty of Science, University of Malaya, 50603 Kuala Lumpur, Malaysia. M. HAMDI, Supervisor, is with the Center of Advanced Manufacturing and Material Processing, University of Malaya, 50603 Kuala Lumpur, Malaysia.

Manuscript submitted February 29, 2012.
Article published online January 9, 2013

ges of this method compared to other methods include the following: (1) rapid reaction rate, (2) controllable reaction conditions, (3) the ability to produce uniformly shaped nanostructures, (4) narrow size distributions, and (5) high porosities.[7,31–34]

Based on the influence of solvent type and irradiation time on the morphology and purity of monetite, we present a sonochemical method for the preparation of monetite in an aqueous solution that contains calcium chloride and sodium dihydrogen phosphate in the presence of *N*,*N*-dimethylformamide (DMF) and ethylene glycol (EG) solvents. The objective of this study is to investigate the effects of the ultrasonic irradiation time and various ratios of DMF on the morphology and crystallization of the resulting monetite.

II. MATERIALS AND METHODS

A. *Synthesis of Monetite*

Commercial analytical grade reagents, including calcium chloride ($CaCl_2$, Sigma Aldrich Co.) and sodium dihydrogen phosphate (NaH_2PO_4, Sigma Aldrich Co.), were used as starting materials. EG (Merck Co.), DMF (J.T. Baker Co.), and deionised water (DI) were used as solvents. The volume of the solvent mixture was maintained at 30 mL for the duration of the process. In the first step, 0.066 g of $CaCl_2$ and 0.049 g of NaH_2PO_4 were added into a solvent mixture of water and EG with a volume ratio of 1:1 (WE). Then, different ratios of WE/DMF (1:0, 1:4, 1:2, 1:1, 2:1, and 1:4) were added dropwise into the solution and vigorously stirred for 1 hour. In the second step, the solution was sonicated using high intensity ultrasonic radiation through direct immersion (Misonix Sonicator S-4000, USA, 20 kHz) for various lengths of time (10, 20, 30, 40, and 60 minutes) at 298.15 K (25 °C). The products were separated from the solution by centrifuging at 8000 rpm, and they were then washed four times with DI and ethanol and dried at 323.15 K (50 °C) for 1 hour.

B. *Characterization*

X-ray diffraction (XRD) patterns of the samples were recorded on an Analytical Empyrean X-ray diffractometer with Cu-K_α radiation (λ = 1.54178 Å), which was operated at 45 kV and 30 mA with a step size of 0.026 deg and a scanning rate of 0.1 deg/s^{-1} in a 2θ range from 10 to 70 deg. The weight of the powder was constant in all the tests. The morphology of the synthesized powders was examined using a high resolution FEI Quanta 200F (FEI, USA) field emission scanning electron microscope (FESEM). Fourier transform infrared spectroscopy (FTIR) measurements were performed with a Perkin Elmer Spectrum 400 spectrometer without using the KBr disk method. The spectra were obtained over a wavenumber range of 4000 to 400 cm^{-1}. Statistical analysis (average thickness of the plates) was performed using a statistical software package version 19 (SPSS Institute, Chicago, IL) with the assistance of image analysis software.

III. RESULTS AND DISCUSSION

The XRD patterns of the monetite powder synthesized from the mixture of solvents, including water (5 mL), EG (5 mL), and DMF (20 mL), at a pH of 4.3 are shown in Figure 1. After the reaction was completed, the solution was named SA. The results indicated that the products were a single phase of crystalline monetite with a triclinic

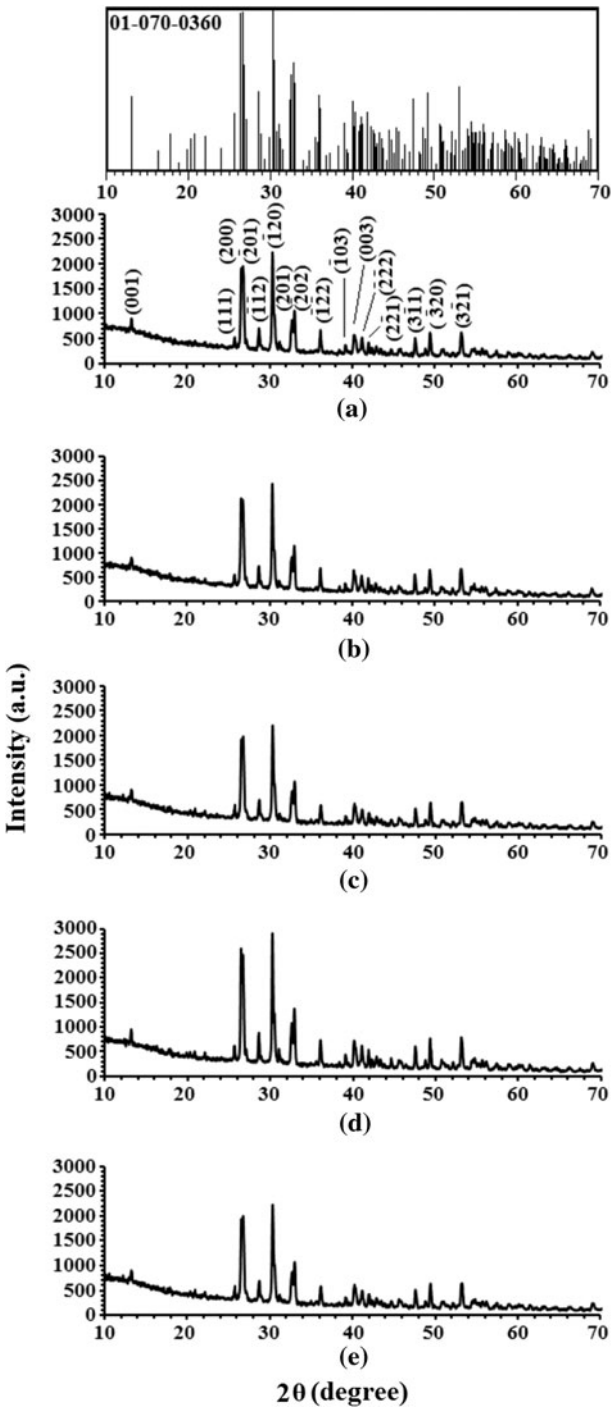

Fig. 1—XRD patterns of samples prepared using different ultrasonic irradiation times: (*a*) 10 min, (*b*) 20 min, (*c*) 30 min, (*d*) 40 min, and (*e*) 60 min.

structure and high-phase purity (ICDD #70-0360). No other diffraction peaks were observed other than the main peaks that corresponded to the monetite structure. Clearly, with ultrasonic irradiation, the monetite peak intensity is significantly increased, and the texture becomes sharp, which indicates that the sample can be well crystallized with the aid of ultrasonic irradiation. The peak intensity in the XRD pattern of the powder synthesized using the sonochemical method is different from that of the previous report. Ruan *et al.*[7] stated that the strongest peak in the XRD pattern of the products synthesized *via* ultrasonic irradiation was (200) observed in the presence of a CTAB surfactant aqueous solution, whereas in this study, the strongest peak intensity corresponded to the ($\bar{1}20$) lattice plane when an aqueous mixture of EG and DMF was used. Comparing the XRD patterns in this work with those of previous reports most likely confirms that the mixture of solvents influences the XRD peak intensity. In addition, many researchers believe that resorbability and bioactivity are two significant characteristics of bioceramics. Furthermore, crystallinity is an important factor that can potentially affect the product resorbability and bioactivity in biomedical applications.[35,36] To obtain the percentage of crystallinity in the sample,[37] its amorphous content was determined by calculating the ratio of the amorphous area of the X-ray diffractogram to the total area. The amorphous area refers to the area of the diffractogram that does not contain diffraction peaks. This process involves the following steps:

Step 1: Smoothing the diffraction pattern using the Savitzky–Golay method.
Step 2: Creating a baseline for the diffractogram using the Sonnefield–Visser method.
Step 3: Computing the integral area, which includes only the crystalline fraction of the material.
Step 4: Computing the total area of the diffractogram by performing this entire operation without creating a baseline.
Step 5: Determining the percent crystallinity by multiplying the ratio of the crystalline area to the total area by 100.

The results in Table I show that the monetite powder synthesized under ultrasonic irradiation for 10 minutes (Figure 1(a)) has a crystallinity of 19.12 ± 0.75 pct, which increases to 22.11 ± 0.45 pct for the sample obtained under ultrasonic irradiation for 40 minutes (Figure 1(d)); furthermore, the crystallinity decreased from 22.11 ± 0.45 to 19.23 ± 0.48 pct as the ultrasonic time was extended from 40 to 60 minutes. These results indicate that ultrasonic irradiation plays a central role in determining the crystallinity of the products obtained using the sonochemical method.

Figure 2 presents the positions of the characteristic bands at 2810, 1633, 1124, 1060, 991, 882, and 535 cm^{-1} in the FTIR spectra, which are assigned as the stretching and bending of phosphate, the stretching mode of the hydroxyl (OH) group, and the water bending mode of monetite. There are sharp and well-separated peaks at approximately 535 to 1124 cm^{-1}, which are all attributed to the PO_4^{3-} group. The peaks at approximately

Table I. Percent Crystallinity of the Sonochemically Synthesized Monetite at Different Times

ST*	Percent Crystallinity (Different Sonication Time)
10	19.12 ± 0.75
20	19.31 ± 0.66
30	19.59 ± 0.58
40	22.11 ± 0.45
60	19.23 ± 0.48

*Sonication time.

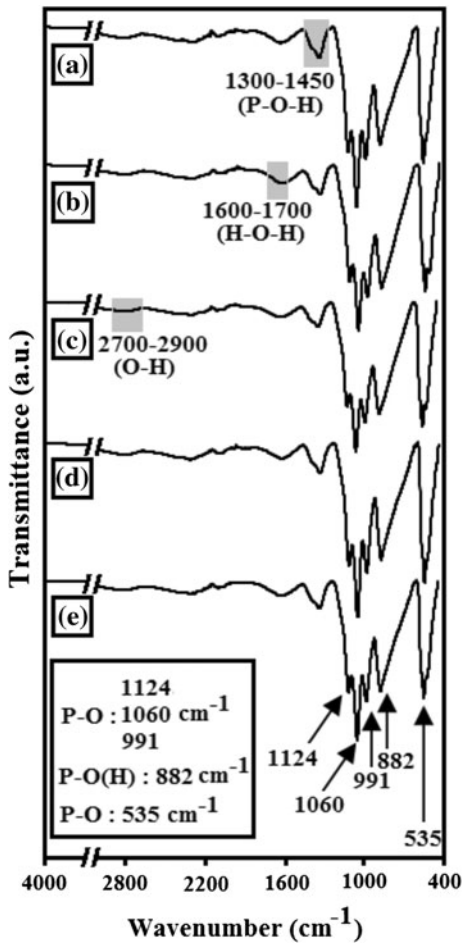

Fig. 2—FT-IR spectra of samples prepared using different ultrasonic irradiation times: (*a*) 10 min, (*b*) 20 min, (*c*) 30 min, (*d*) 40 min, and (*e*) 60 min.

1060 (v_3PO_4), 991(v_1PO_4), and 1124 cm^{-1} were assigned to P-O stretching. The band at 882 cm^{-1} was assigned to the P-O(H) stretching vibrations of the acidic phosphate group (HPO_4^{2-}). The band located at approximately 535 cm^{-1} was attributed to P-O bending (v_4PO_4). The broad peak at 1300 to 1450 cm^{-1} corresponds to the P-O-H in-plane bending, whereas the broad band at approximately 1633 cm^{-1} is associated with the H-O-H bending and the rotation of the residual free water. The broad band at approximately 2810 cm^{-1} was assigned to

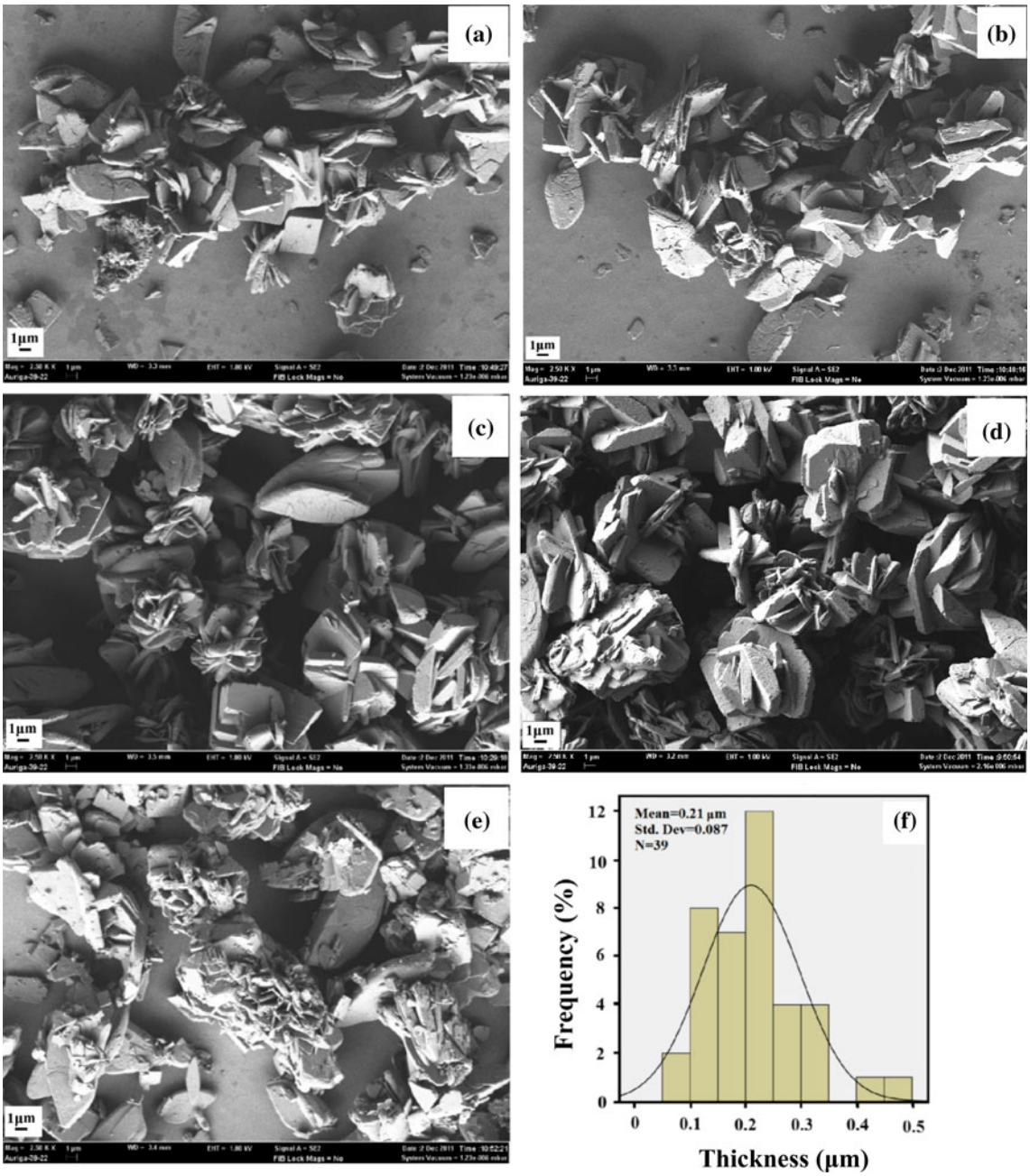

Fig. 3—FESEM images of samples prepared using a volume ratio of WE/DMF of 1:2 with different sonication times: (*a*) 10 min, (*b*) 20 min, (*c*) 30 min, (*d*) 40 min, and (*e*) 60 min; (*f*) average thickness after 40 min.

the O-H stretching vibration band of HPO_4^{2-}.[9,19,38–44] The large separation of peaks is another indicator of a well-crystallized monetite phase.[7,45] These results are in good agreement with the X-ray diffraction analysis.

Figure 3 presents the FESEM images of the SA solution after various durations of sonochemical irradiation. The FESEM results reveal that the morphology of the synthesized monetite powder changes slightly from plate-like to a plate-like combination (flower-like) as the sonication time increases. As shown in Figure 3(a), the dominant morphology is mostly plate-like and only a minor portion is non-plate-like in comparison with Figure 3(d), in which the dominant morphology is a plate-like combination (flower-like). Thus, it is reasonable to make the following conclusion: The ultrasonic irradiation time not only affects the crystallinity of the samples but also has an influence on the morphology of the samples. Note that throughout the entire sonication time, the plates maintained their straight edges, uniform widths, and rather well-defined smooth surfaces. In addition, it was observed that the dimensions of the products obtained *via* the sonochemical method varied with the ultrasonication time. It is particularly significant that no obvious changes can be observed in the two-axis dimension (length and width). The average plate thickness for 40 minutes of ultrasonication is 210 ± 87 nm

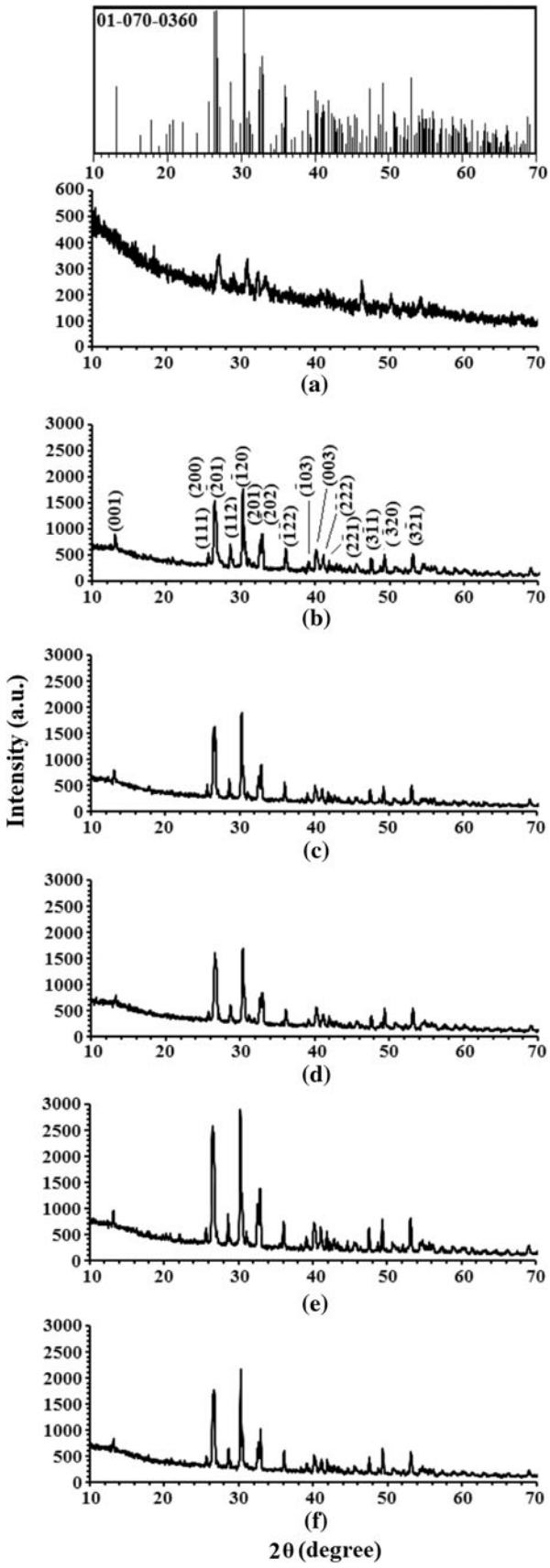

Fig. 4—XRD patterns of samples prepared with different ratios of WE/DMF: (*a*) 1:0, (*b*) 4:1, (*c*) 2:1, (*d*) 1:1, (*e*) 1:2, and (*f*) 1:4.

Table II. Percent Crystallinity of the Sonochemically Synthesized Monetite at Different Ratios of WE/DMF

WE/DMF	Percent Crystallinity (Different Ratio of DMF)
1:0	7.08 ± 0.71
4:1	15.45 ± 0.48
2:1	15.78 ± 0.25
1:1	17.08 ± 0.33
1:2	22.11 ± 0.45
1:4	16.34 ± 0.48

(Figure 3(f)). The results from previous studies[7,46] have shown that the samples were 5 to 50 μm in width, 2 μm in length, and 100 to 200 nm or 0.5 to 2 μm in thickness. The thickness of the samples, which is approximately 100 nm to 900 nm, decreases as the sonication time increases. The comparison between Figures 3(d) and (e) (sonication times of 40 and 60 minutes, respectively) reveals that increasing the sonication time from 40 to 60 minutes has a destructive effect on the morphologies of the samples. From the FESEM results, it can be concluded that 40 minutes of sonication time is optimal for the synthesis of a plate-like combination morphology (flower-like).

The XRD patterns of synthesized powders fabricated with different DMF ratios and a constant WE ratio of 1:1 at 40 minutes of sonication are shown in Figure 4. The strongest peaks in the diffractograms are the lattice planes of $(\bar{1}20)$ and (200). Figure 4(a) presents the XRD pattern of the powder synthesized in a water/EG mixture without DMF. Ma *et al.*[7] reported the synthesis of monetite with excellent crystallinity in a water/EG mixture using a microwave-assisted method, whereas the crystallinity of the powder synthesized in the presence of water/EG using the sonication method was very low. Therefore, it can be concluded that DMF has a crucial role in the synthesis and on the crystallinity of the monetite powder prepared *via* sonication. The comparison of the XRD patterns of products without (Figure 4(a)) and with DMF (Figure 4(b), with a WE:DMF ratio of 4:1) clearly reveals the effect of DMF on the synthesized powder. Figures 4(b) through (f) demonstrate the effect of different DMF concentrations on the product crystallinity. Note that sharp monetite peaks appear in the XRD pattern as the DMF content increases. Furthermore, the peak intensity increases when the ratio is increased to 1:2 (Figure 4(e)) and then decreases when the ratio is changed to 1:4 (Figure 4(f)). The crystallinities of the powders synthesized with various WE/DMF ratios are given in Table II. It is evident that as the DMF ratio increases, the crystallinity increases and is maximized for the ratio of 1:2 (22.11 ± 0.45 pct). Therefore, the results confirm that the appropriate ratio of WE to DMF is an important factor in the formation of a suitable monetite crystal. The experimental results clearly demonstrate that the optimum WE to DMF ratio for obtaining adequate crystallinity is 1:2. The reason for this phenomenon and the effect of DMF can be clarified with the following scheme:

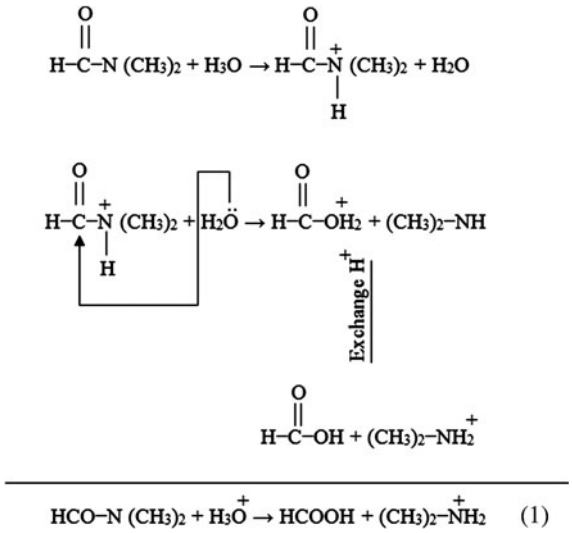

The pH was 4.3 after the aforementioned solution (WE:DMF 1:2) was prepared. It was hypothesized that when the pH<4.5, $(CH_3)_2NH_2^+$ will be formed due to the reaction between DMF and H_3O^+. The product of this reaction can provide a basic condition for the nucleation and growth of the monetite. It was observed that long irradiation times increased the temperature of the reaction media, which consequently increased the reaction rate. The XRD results reveal that the crystallinity is increased when the ratio of WE/DMF is changed from 1:0 to 1:2. In addition, the concentration of $(CH_3)_2NH_2^+$ will also increase as the concentration of DMF is increased. Note that there is a limitation for increasing the DMF ratio and producing $(CH_3)_2NH_2^+$. This limitation is the pH, which has a special substantial role in the conversion of DMF to $(CH_3)_2NH_2^+$. In addition, when the concentration of DMF is too high, sufficient monetite crystals cannot be obtained because

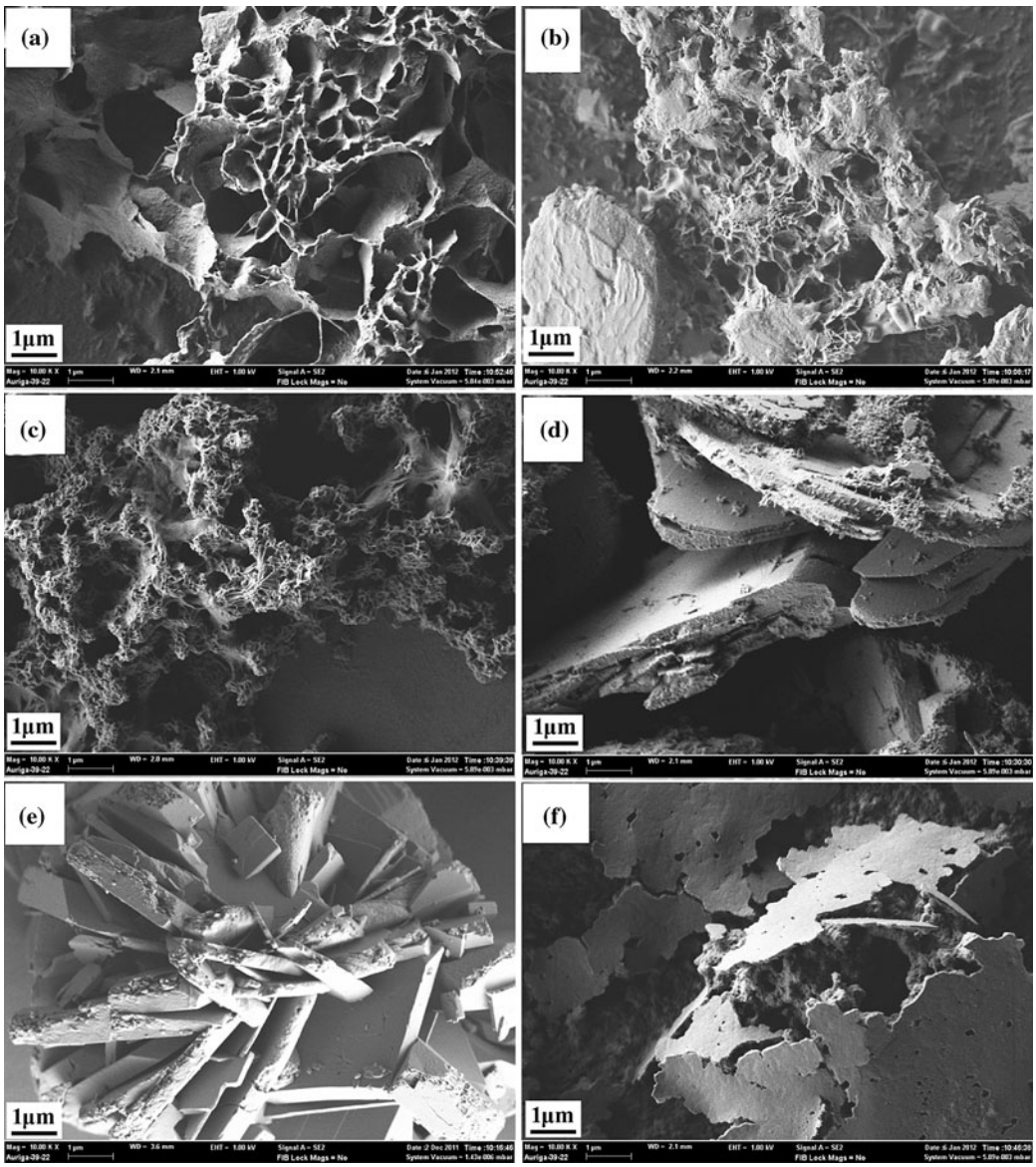

Fig. 5—FESEM images of samples prepared with different ratios of WE/DMF: (*a*) 1:0, (*b*) 4:1, (*c*) 2:1, (*d*) 1:1, (*e*) 1:2, and (*f*) 1:4.

of the rapid nucleation and growth of monetite, as previously reported.[21] Therefore, an appropriate amount of DMF is a key factor in the formation of monetite. Moreover, other researchers maintain that the addition of viscous EG liquid to the reaction system may influence the formation of crystals by decreasing the diffusion rates of the reactant ions.[5,23] The EG molecule, which has two hydroxyl groups, is polar and plays a crucial role in mediating the crystal phase and the product morphology. The diffusion of Ca^{2+} and HPO_4^{2-} ions and rapid nucleation are restrained due to the high viscosity of EG at room temperature. When the temperature is elevated by increasing the processing time, the viscosity of the EG is rapidly decreased, while the polarization of EG and water molecules under the rapidly changing sonication frequency could facilitate the anisotropic growth of the monetite plates. It was observed that the higher crystallinity of the synthesized monetite depends on the concentration of DMF and the ultrasonic irradiation time, which is evident from the FESEM and XRD results.

Figure 5 presents the effect of different concentrations of DMF on the morphology of the monetite powder synthesized with 40 minutes of ultrasonic irradiation time. The morphology clearly transforms as the DMF to WE ratio changes. Figure 5(a) presents the FESEM image of a nanowall morphology in the absence of DMF, whereas Figures 5(b) through (d) depict the increase in the nanowall thickness and agglomeration. The FESEM image in Figure 5(d) illustrates the complete plate shapes of the monetite with thicker walls and a rough surface. The results also indicate that well-developed crystals of monetite were obtained as a result of increased quantities of DMF when all other conditions were held constant (Figure 5(e)). It was observed that increasing the DMF ratio from 1:2 (Figure 5(e)) to 1:4 (Figure 5(f)) had a destructive effect on the morphology, which was characterized by the formation of nanosheets, as shown in Figure 5(f). These results confirm that solvent mixtures of WE and DMF are favorable for the synthesis of monetite with various types of morphologies.

IV. CONCLUSIONS

In summary, the present work reports on the synthesis of monetite powder with a plate-like morphology and with plate-like combination (flower-like) morphology using sonochemical treatment with $CaCl_2$ and NaH_2PO_4 in the presence of the ternary H_2O/EG/DMF solvent system. The syntheses were performed with various sonication times, different DMF ratios, and a constant ratio of EG/water (1:1). The morphology and crystallinity of the product were found to vary with different sonication times and DMF ratios. DMF influences the release of $(CH_3)_2NH_2^+$ and, consequently, provides a basic condition for the nucleation and growth of monetite. The results indicate that the optimum crystal phase is obtained after 40 minutes of sonication time and demonstrates a flower-like morphology and an average thickness of 210 ± 87 nm. Finally, it was determined that the sonication time and the solvent concentrations have significant effects on the morphology and crystallinity of the product.

ACKNOWLEDGMENTS

The authors wish to thank P. M. Tehrani for valuable discussion. This work has been supported by the University of Malaya, Grant No: HIR F00004-21001 and FRGS grant number FP039 2010B and RG181 12SUS.

REFERENCES

1. M. Vallet-Regí: *C. R. Chim.*, 2010, vol. 13, pp. 174–85.
2. S.V. Dorozhkin: *Biomaterials*, 2010, vol. 31, pp. 1465–85.
3. S. Baradaran, M. Hamdi, and I.H. Metselaar: *Adv. Appl. Ceram.*, 2012, vol. 111, pp. 367–73.
4. Y.-S. Hsu, E. Chang, and H.-S. Liu: *Ceram. Int.*, 1998, vol. 24, pp. 249–54.
5. M.G. Ma, Y.J. Zhu, and J. Chang: *J. Phys. Chem. B*, 2006, vol. 110, pp. 14226–30.
6. S. Jinawath, D. Pongkao, W. Suchanek, and M. Yoshimura: *Int. J. Inorg. Mater.*, 2001, vol. 3, pp. 997–1001.
7. Q. Ruan, Y. Zhu, Y. Zeng, H. Qian, J. Xiao, F. Xu, L. Zhang, and D. Zhao: *J. Phys. Chem. B*, 2009, vol. 113, pp. 1100–06.
8. K. Wei, C. Lai, and Y. Wang: *J. Mater. Sci.*, 2007, vol. 42, pp. 5340–46.
9. A.V. Zavgorodniy, R.S. Mason, R.Z. LeGeros, and R. Rohanizadeh: *Surf. Coat. Technol.*, 2012, vol. 206, pp. 4433–38.
10. R.R. Kumar, K. Prakash, K. Yennie, P. Cheang, and K. Khor: *Key Eng. Mater.*, 2005, vol. 284, pp. 59–62.
11. K. Li and S.C. Tjong: *IEEE*, 2010, pp. 856–57.
12. H. Zhang, K. Zhou, Z. Li, and S. Huang: *J. Phys. Chem. Solids*, 2009, vol. 70, pp. 243–48.
13. A. Milev, G. Kannangara, and B. Ben-Nissan: *Key Eng. Mater.*, 2002, vol. 240, pp. 481–84.
14. T. Watanabe, G. Kawachi, M. Kamitakahara, K. Kikuta, and C. Ohtsuki: *J. Ceram. Soc. Jpn.*, 2009, vol. 117, pp. 759–64.
15. S.P. Sun, M. Wei, J.R. Olson, and M.T. Shaw: *Rheol. Acta*, 2011, vol. 50, pp. 65–74.
16. J.H. Yang, K.H. Kim, C.K. You, T.R. Rautray, and T.Y. Kwon: *J. Biomed. Mater. Res. B*, 2011, vol. 99B, pp. 150–57.
17. P.M.S.L. Shanthi, M. Ashok, T. Balasubramanian, and A. Uthirakumar: *Proc. SPIE*, 2009, vol. 7403, p. 74030K.
18. E. Fujii, K. Kawabata, Y. Nakazaki, Y. Tanizawa, Y. Shirosaki, S. Hayakawa, and A. Osaka: *J. Ceram. Soc. Jpn.*, 2011, vol. 119, pp. 116–19.
19. B. Jokic, M. Mitric, V. Radmilovic, S. Drmanic, R. Petrovic, and D. Janackovic: *Ceram. Int.*, 2011, vol. 37, pp. 167–73.
20. H. Zhang and B.W. Darvell: *J. Am. Ceram. Soc.*, 2011, vol. 94, pp. 2007–13.
21. M.G. Ma and J.F. Zhu: *Eur. J. Inorg. Chem.*, 2009, vol. 2009, pp. 5522–26.
22. M.G. Ma, Y.J. Zhu, and J. Chang: *Mater. Lett.*, 2008, vol. 62, pp. 1642–45.
23. F. Chen, Y.J. Zhu, K.W. Wang, and K.L. Zhao: *CrystEngComm*, 2010, vol. 13, pp. 1858–63.
24. S. Jalota, A.C. Tas, and S.B. Bhaduri: *Int. J. Mater. Res.*, 2004, vol. 19, pp. 1876–81.
25. M. Djosic, V. Miskovic-Stankovic, Z. Kacarevic-Popovic, B. Jokic, N. Bibic, M. Mitric, S. Milonjic, R. Jancic-Heinemann, and J. Stojanovic: *Colloids Surf. A*, 2009, vol. 341, pp. 110–17.
26. G. Bezzi, G. Celotti, E. Landi, T. La Torretta, I. Sopyan, and A. Tampieri: *Mater. Chem. Phys.*, 2003, vol. 78, pp. 816–24.
27. X.D. Kong, X.D. Sun, J.B. Lu, and F.Z. Cui: *Curr. Appl. Phys.*, 2005, vol. 5, pp. 519–21.
28. J. Zhu, Y. Koltypin, and A. Gedanken: *Chem. Mater.*, 2000, vol. 12, pp. 73–78.
29. D.V. Pinjari and A.B. Pandit: *Ultrason. Sonochem.*, 2011, vol. 18, pp. 1118–23.

30. J.H. Bang and K.S. Suslick: *Adv. Mater.*, 2010, vol. 22, pp. 1039–59.
31. A.Y. Baranchikov, V.K. Ivanov, and Y.D. Tretyakov: *Russ. Chem. Rev.*, 2007, vol. 76, pp. 133–51.
32. A. Gedanken: *Curr. Sci.*, 2003, vol. 85, pp. 1720–22.
33. V.S. Manoiu and A. Aloman: *Sci. Bull. B*, 2010, vol. 72, pp. 179–86.
34. H. Wang, J.J. Zhu, J.M. Zhu, and H.Y. Chen: *J. Phys. Chem. B*, 2002, vol. 106, pp. 3848–54.
35. Q. Hu, Z. Tan, Y. Liu, J. Tao, Y. Cai, M. Zhang, H. Pan, X. Xu, and R. Tang: *J. Mater. Chem.*, 2007, vol. 17, pp. 4690–98.
36. S. Overgaard, U. Bromose, M. Lind, C. Bunger, and K. Soballe: *J. Bone Jt. Surg. Br. Vol.*, 1999, vol. 81, pp. 725–31.
37. K. Prasad, D.V. Pinjari, A.B. Pandit, and S.T. Mhaske: *Ultrason. Sonochem.*, 2010, vol. 17, pp. 697–703.
38. X. Xin-bo, Z. Xie-rong, Z. Chun-li, L. Ping, and F. Yun-bo: *Surf. Coat. Technol.*, 2009, vol. 204, pp. 115–19.
39. X.X. Bo, Z.C. Li, Z.X. Rong, L. Ping, F.Y. Bo, T.H. Lin, and X.S. Hui: *Mater. Sci. Eng. C*, 2009, vol. 29, pp. 2019–23.
40. S. Mandel and A.C. Tas: *Mater. Sci. Eng. C*, 2010, vol. 30, pp. 245–54.
41. M. Rajkumar, N.M. Sundaram, and V. Rajendran: *Int. J. Eng. Sci.*, 2010, vol. 2, pp. 2437–44.
42. L. Wang and J.L. Luo: *Metall. Mater. Trans. A*, 2011, vol. 42A, pp. 3255–64.
43. E. Mohammadi Zahrani, M. Fathi, and A. Alfantazi: *Metall. Mater. Trans. A*, 2011, vol. 42A, pp. 3291–3309.
44. T. Nakano, Y. Umakoshi, and A. Tokumura: *Metall. Mater. Trans. A*, 2002, vol. 33A, pp. 521–28.
45. G. Xu, I.A. Aksay, and J.T. Groves: *J. Am. Chem. Soc.*, 2001, vol. 123, pp. 2196–2203.
46. H. Ito, Y. Oaki, and H. Imai: *Cryst. Growth Des.*, 2008, vol. 8, pp. 1055–59.